Chinese Chemical Letters 32 (2021) 3090–3094

Contents lists available at ScienceDirect

Chinese Chemical Letters

journal homepage: www.elsevier.com/locate/cclet

Communication

Laser-assisted synthesis of cobalt@N-doped carbon nanotubes decorated channels and pillars of wafer-sized silicon as highly efficient three-dimensional solar evaporator

Yiwei Zhao[a,b,1], Haifeng Yuan[b,1], Xiaofei Zhang[a], Guobin Xue[b], Jiebin Tang[b], Yuke Chen[b], Xiaoli Zhang[c], Weijia Zhou[b,*], Hong Liu[a,b,**]

[a] State Key Laboratory of Crystal Materials, Shandong University, Ji'nan 250100, China
[b] Collaborative Innovation Center of Technology and Equipment for Biological Diagnosis and Therapy in Universities of Shandong, Institute for Advanced Interdisciplinary Research (iAIR), University of Jinan, Ji'nan 250022, China
[c] School of Materials Science and Engineering, Zhengzhou University, Zhengzhou 450001, China

ARTICLE INFO

Article history:
Received 19 January 2021
Received in revised form 19 February 2021
Accepted 24 February 2021
Available online 26 February 2021

Keywords:
Laser process
Carbon nanotubes
Silicon pillars
Photothermal conversion
Water evaporation

ABSTRACT

The Co@NCNTs/Si pillars with channels is assemble to a suitable pure water gathering device, which is applied in seawater desalination and sewage purification to produce pure water by utilizing solar energy. High-efficiency utilization of solar energy to generate water vapor is popular, recyclable, and environmentally friendly for seawater desalination and sewage purification, helping to alleviate the global water shortage crisis. Here, we report an efficient and simple method to prepare a three-dimensional (3D) evaporator for steam generation by harnessing the power of the sun. This evaporation is composed of one-dimensional (1D) cobalt embedded and nitrogen doped carbon nanotubes (Co@NCNTs) and 3D silicon pillars array structure (Si pillars). The Co@NCNTs/Si pillars shows a wide light absorption range provided by carbon nanotubes and a long light absorption path because of the silicon pillars. The surface temperature of the sample rises rapidly in 1.5 min and exceed 80 °C under solar illumination of one sun. The water evaporation can be high as 1.21 kg m^{-2} h^{-1} under one sun irradiation (1 kW/m^2) with the energy efficiency up to 82.4%. This scalable Co@NCNTs/Si pillars can prepare pure water from seawater and sewage, where the removal rate of ions in seawater and pollutants in sewage is similar to 100%. Based on our research, this multistage three-dimensional structure is a simple and efficient novel photothermal material for extensive seawater desalination and sewage purification.

Aiming at the water shortage problem and energy crisis, solar steam generation was considered as an advanced technology of the future for seawater desalination and waste water purification [1,2]. Compared with traditional desalination technologies, its biggest advantages were sustainable, low energy consumption and environmentally friendly as solar energy was the only input energy [3]. Increasing the solar-thermal conversion efficiency, reducing heat loss were critical factors for practical implementation of the solar-driven interfacial evaporation system [4]. According to the above factors, several measures were proposed through developing effective photothermal materials [5], reducing heat loss with heat concentration [6,7], providing effect water/steam transmission interface and extending durability [8,9]. Carbon materials such as carbon nanotubes [10,11], graphene [12–14], carbon black [15,16], were extensively used as photothermal materials in generating solar steam because of the high solar absorption efficiency and photothermal conversion capability [17]. A variety of substrate materials such as wood [18,19], polymer [20], were combined with carbon materials to take advantage of the photothermal properties of carbon materials [21]. Moreover, 3D solar-energy evaporator could also maintain structural stability and salt resistance under long-time test conditions, indicating that the evaporator could be used for water evaporation with durability [22]. For instance, Tang *et al.* selected wood as basement and built an evaporator by adjusting the height of the wood floated on the water and regulating the hydrophilicity of charred wood surfaces achieving a high-water evaporating rate of 1.93 kg m^{-2} h^{-1} under

* Corresponding author.
** Corresponding author at: State Key Laboratory of Crystal Materials, Shandong University, Ji'nan 250100, China.
E-mail addresses: ifc_zhouwj@ujn.edu.cn (W. Zhou), hongliu@sdu.edu.cn (H. Liu).
[1] These authors contributed equally to this work.

https://doi.org/10.1016/j.cclet.2021.02.056
1001-8417/

one sun illumination (1 kW/m^2) [23]. Meanwhile, the three-dimensional structure of the substrate could reduce heat loss and promote heat concentration [24–26]. All of the above material characteristics were helpful to enhance photothermal water evaporative performance. Nevertheless, capturing solar energy and converting it into heat for efficient utilization remained a challenge.

In this work, silicon wafer was selected as the substrate, orderly three-dimensional silicon pillars and water transmission channels were constructed on silicon wafer by a controllable laser etching process, which was a typical material processing method [27]. The 3D silicon arrays were covered with cobalt embedded and nitrogen doped carbon nanotubes samples (Co@NCNTs/Si pillars) by calcining dicyandiamide (DCDA) and cobaltous silicate which was loaded on silicon pillars by reacting with cobalt-ammonia solution. The 3D silicon pillars enhanced the light absorbability and reduced light reflection by enlarging the surface area, and extending the light route for repeated reflections. In addition, the Co@NCNTs was a kind of photothermal material with wide spectral absorption range. Under one sun illumination, the superficial temperature of the sample rose hastily in 1.5 min and exceed 80 °C. We floated the sample on the water and assembled it into a simple water evaporator, which would be widely used in seawater desalination and wastewater purification. The daily evaporation achieved 1.21 kg m^{-2} h^{-1}, and the energy efficiency could come to 82.4% with no additional thermal management accessories. The rejection rate of metal ions and organic dyes was close to 100%.

Ammonium chloride (NH_4Cl), ammonia ($NH_3{\cdot}H_2O$, 25 wt%), cobalt chloride hexahydrate ($CoCl_2{\cdot}6H_2O$), DCDA ($C_2H_4N_4$), sulfuric acid (H_2SO_4), hydrofluoric acid (HF, 35%), hydrogen peroxide (H_2O_2, 35%) were bought from Sinopharm Chemical Reagent Co., Ltd. P-Si-(100) with 0.003–0.005 Ω cm resistivity was purchased from Tianjin Semiconductor Research Institute Co., Ltd., and Ar gas (99.99%) which was obtained from Jining Gases (Shandong, China). All reagents were used without further purification. Deionized water was supplied with a Barnstead Nanopure Water System (18.2 MΩ cm) and was employed to configurate the total solutions.

The silicon pillars were constructed selecting silicon wafer as basement by optical fiber laser system (LSF20D, Hgtech Laser) with a laser wavelength of 1064 nm and pulse duration of 20 μs in air atmosphere. A circle scan mode with the repetition rate of 20 kHz, pulse energy of 0.1 mJ, scanning spacing of 0.05 mm and scanning speed of 2000 mm/s was used. Specifically, connecting a computer to the laser system, using a software (named EzCad2) to set the experimental parameters, and draw the patterns with circle fitting mode, the silicon pillars were generated. Finally, silicon pillars were etched with 5 wt% HF aqueous solution for 30 min under room temperature to remove the oxide layer on the surface of silicon pillars.

The silicon pillars were cut into a circle with the diameter of 35 mm and placed in a reaction kettle with 25 mL prepared cobalt-ammonia transparent solution (Co^{2+}, 0.3 mmol; NH_4Cl, 10 mmol; $NH_3{\cdot}H_2O$, 1 mL) [28]. The samples were heated in an oven at 90 °C for 6 h. The silicon pillars reacted with cobalt-ammonia solution and formed a layer of $Co_3Si_2O_5(OH)_4$ nanosheets on the surface of silicon pillars named $Co_3Si_2O_5(OH)_4$/Si pillars. For the synthesis of Co@NCNTs/Si pillars, plenty of DCDA was spread evenly over the bottom of a crucible, and the $Co_3Si_2O_5(OH)_4$/Si pillars was placed on the top at a slant. After sealed and wrapped with copper foil, the crucible was placed into the center of the tube furnace and heated at 750 °C for 2 h under Ar gas condition, the Co@NCNTs was prepared on silicon pillars named Co@NCNTs/Si pillars.

To characterize the morphology and elemental distribution of materials, Field emission scanning electron microscope (FESEM, HITACHI regulus 8100) and high-resolution transmission electron microscopy (HRTEM, Thermo Fischer Talos F200x) were adopted. In addition, X-ray diffractometer (XRD, Cu Kα radiation, λ = 0.15406 nm, Rigaku Ultima IV, JPN) and X-ray photoelectron spectra (XPS, AXIS SUPRA, Kratos) were employed to study the element composition and crystal structure. UV–vis-NIR spectrophotometer (UH4150, Hitachi High-Technologies Corporation) and Fotric 226 Thermal Imaging Camera were used to exam the photothermal properties of the samples. All temperature profiles were recorded as real-time videos, and the exact temperature measurements of each individual frame were performed on software (FOTRIC, AnalyzIR).

A beaker with an opening diameter of 40 mm was prepared to serve as a container for water. Simulated solar with the light intensity kept at 1 kW/m^2 (one sun) was provided by a xenon lamp (CEL-HXF300, 300 W, CEAULIGHT), A foam was used to float the sample on the water. The exposed area of the sample used in the experiment was a square with a side length of 18 mm. The sample floated on the water with foam was illuminated vertically by simulated sunlight. An electronic analytical balance linked with a computer was used to record the mass change of the breaker in real time caused by the photothermal evaporation. All tests were performed at an environment temperature of 24 °C ± 0.5 °C and a relative humidity of 50%.

The formula (1) was used to calculate the evaporation rate (υ_e) of water during the experiment [17]:

$$\upsilon_e = dm/(S \times dt) \quad (1)$$

where dm was the weight change of the breaker, S was the area of the sample irradiated by the simulated sunlight (square area with a side length of 18 mm), and dt was the irradiated time.

The synthetic procedure of Co@NCNTs/Si pillars was showed in Fig. 1a. First, the silicon wafer with pillars and channels were got by laser engraving in the air (Fig. 1a-A). The surface morphology of silicon pillars was shown in Fig. 1b. After reacted with cobalt-ammonia solution, the silicon wafer, with pillars and channels, were covered with a layer of cobalt silicate ($Co_3Si_2O_5(OH)_4$) nanosheets as shown in Fig. 1c (Fig. 1a-B). After annealing $Co_3Si_2O_5(OH)_4$/Si pillars with DCDA, Co nanoparticles embedded and N-doped carbon nanotubes (Co@NCNTs) on Si pillars (Co@NCNTs/Si pillars) were gained (Fig. 1d), that originated from cobalt silicate was reduced to cobalt metal to catalyze the development of NCNTs (Fig. 1a-C) [29–31]. When the amount of DCDA added was adjusted, the morphology of corresponding carbon nanotubes was different. When the amount of DCDA added was small (20 mg), the carbon nanotubes formed were few and short, and there were a few unreacted cobalt silicate nanosheets

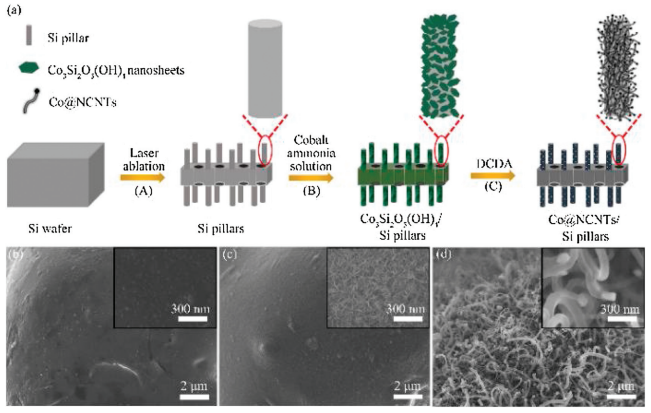

Fig. 1. (a) Scheme of synthetic procedure of Co@NCNTs/Si pillars. SEM images of (b) silicon pillars, (c) $Co_3Si_2O_5(OH)_4$/Si pillars, (d) Co@NCNTs/Si pillars and their corresponding detail views of the surface.

remained on the silicon pillars (Fig. S1a in Supporting information). To some extent, this could be inferred from the growth process of carbon nanotubes, that was, the cobalt silicate nanosheet was reduced to the metallic cobalt nanoparticles as the precursor, and then the metallic cobalt nanoparticles as the catalyst promoted the formation of carbon nanotubes [32]. When the amount of DCDA was sufficient (40 mg), the corresponding carbon nanotubes became longer and more numerous. Basically, the silicon pillars were completely covered by the carbon nanotubes (Fig. S1b in Supporting information). When excess DCDA was added (60 mg), the nanotubes became longer and thinner (Fig. S1c in Supporting information).

Scanning electron microscopy (SEM) in Figs. 2a–c showed the overall morphology of Co@NCNTs/Si pillars, the channel with the diameter of about 1 mm was observed from the top view (Fig. 2a). The silicon pillars with the diameter of about 50 μm and the height of about 150 μm were observed from the top view (Fig. 2b) and section diagram (Fig. 2c). By magnifying the construction of Co@NCNTs/Si pillars, the Co@NCNTs were distinctly seen with a diameter size of 30–150 nm and a length size of 2–4 μm on the surface of the silicon pillars (Figs. 2d and e). The SEM image of sectional view in Fig. 2f revealed the thickness of prepared Co@NCNTs for 4–6 μm, signifying the tight interface between Co@NCNTs and Si pillars, this was due to the in-situ growth of carbon nanotubes on the silicon surface [32]. The distribution of carbon, nitrogen, silicon and cobalt elements at the interface between Si pillars and the layer of Co@NCNTs were shown in Fig. 2g. These results indicated that the silicon pillars were coated with a layer of cobalt embedded and nitrogen-doped carbon nanotubes. As shown in Fig. S2 (Supporting information), due to the XRD peak strength of the silicon substrate, single characteristic peaks of silicon (JCPDS No. 27-1402) were detected in the sample of Si pillars, $Co_3Si_2O_5(OH)_4$/Si pillars and Co@NCNTs/Si pillars.

In order to research the composition of separated Co@NCNTs, high-resolution transmission electron microscopy (HRTEM) was carried out. The Co@NCNTs with a diameter of 20–30 nm could be distinctly observed in Fig. S3a (Supporting information). The crystal plane spacing of layers was 0.340 nm consistent with the (002) plane of graphite carbon [33,34]. And the nanoparticle wrapped with NCNTs with a lattice distance of 0.204 nm was consistent with the (111) plane of metallic Co (Figs. S3b in Supporting information) [35]. As shown in Fig. S3c and d (Supporting information), N and C elements were uniformly distributed in the nanotube, while the distribution of Co element was encapsulated in the end of nanotube. $Co_3Si_2O_5(OH)_4$ was reduced to cobalt and silicon dioxide under the temperature of 750 °C [36]. A small amount of silicon element distributed on the surface of carbon tube came from silicon dioxide, which was the reduction product of $Co_3Si_2O_5(OH)_4$. The above data showed the favorable preparation of Co@NCNTs on Si pillars.

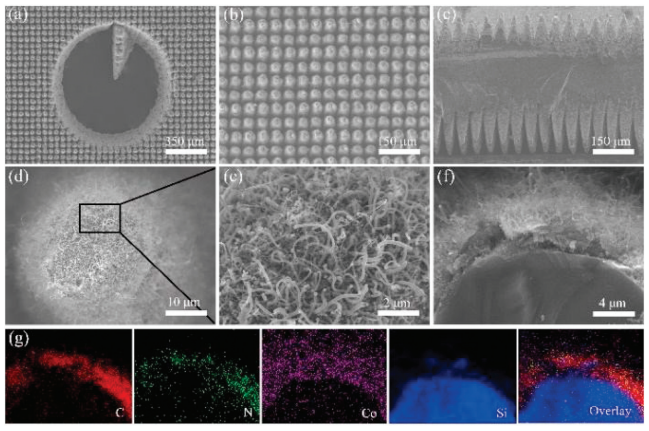

Fig. 2. SEM images of (a) top view of the water channel and Si pillars established on the Co@NCNTs/Si pillars. (b) The top view and (c) side view of Co@NCNTs/Si pillars, and (d) the detail view of Co@NCNTs/Si pillars. (e) The detail view of the Co@NCNTs growing on the Si pillars. (f) The section view of Co@NCNTs/Si pillars. (g) The distribution images of C, N, Co, Si elements and their overlay image on the cross section of the Co@NCNTs/Si pillars.

In order to further explore surface chemical compositions of Si pillars, $Co_3Si_2O_5(OH)_4$/Si pillars and Co@NCNTs/Si pillars, X-ray photoelectron spectra (XPS) measurements were conducted. It could be observed in Fig. S4 (Supporting information), that the survey XPS spectrums of the samples revealed the presence of Si, Co, N and C elements. From the Si 2p XPS spectra (Fig. S5a in Supporting information), the representative peaks at 98.9–104.5 eV of Si 2p electrons were presented in the three samples. What is more, Si^0 was detected in the Co@NCNTs/Si pillars (98.9 eV) and Si pillars (99.6 eV), but not detected in the sample of $Co_3Si_2O_5(OH)_4$/Si pillars. Si 2p electrons at 101.9 eV and 102.9 eV in $Co_3Si_2O_5(OH)_4$/Si pillars consistent with Si^{3+} and Si^{4+} suggested the synthesis of high valent Si on Si pillars after hydrothermal reaction [36,37], as the silicon pillars were uniformly covered by $Co_3Si_2O_5(OH)_4$ nanosheets, and the elemental silicon were not exposed to be detected. When $Co_3Si_2O_5(OH)_4$/Si pillars were calcined with DCDA, the peak of Si° at 98.9 eV could be detected again in the sample of Co@NCNTs/Si pillars. The high-resolution XPS spectra of Co 2p for Si pillars, $Co_3Si_2O_5(OH)_4$/Si pillars and Co@NCNTs/Si pillars were shown in Fig. S5b (Supporting information). For the Si pillars, the Co 2p spectrum was not distinguished, indicating that there was no cobalt element on the sample. After hydrothermal reaction, the high-resolution Co $2p_{3/2}$ and Co $2p_{1/2}$ spectra of $Co_3Si_2O_5(OH)_4$/Si pillars presented the photoelectron signals of Co^{2+} (Co $2p_{3/2}$ at 781.0 eV and Co $2p_{1/2}$ at 797.0 eV) and satellites peaks (Co $2p_{3/2}$ at 784.9 eV and Co $2p_{1/2}$ at 802.7 eV). It indicated that a layer of high valent cobalt was formed on the surface of Si pillars. The high-resolution Co $2p_{3/2}$ and Co $2p_{1/2}$ spectra of Co@NCNTs/Si pillars presented the photoelectron signals of Co° (Co $2p_{3/2}$ at 779.3 eV and Co $2p_{1/2}$ at 794.6 eV), Co^{2+} (Co $2p_{3/2}$ at 780.8 eV and Co $2p_{1/2}$ at 796.2 eV), and two satellites peaks (Co $2p_{3/2}$ at 782.3 eV and Co $2p_{1/2}$ at 803.4 eV) [38], this indicated that after high temperature calcination with DCDA, most of the Co^{2+} in $Co_3Si_2O_5(OH)_4$/Si pillars sample were reduced to Co°. From the C 1s XPS spectra in Fig. S5c (Supporting information), the high-resolution C 1s spectra of the Co@NCNTs/Si pillars sample was divided into two peaks including sp^2-hybridized graphitic carbon atoms with a binding energy of 284.5 eV, and a small signal at higher binding energy (285.6 eV), which was attributed to C—N bonding configurations. Meanwhile, the N 1s spectra of Co@NCNTs/Si pillars sample could be fitted into three peaks at 398.4 eV, 399.0 eV and 400.9 eV (Fig. S5d in Supporting information), respectively. The pyridinic nitrogen with a binding energy of 398.4 eV and pyrrole nitrogen with a binding energy of 399.0 eV could impute the π-conjugated system with a pair of p-electrons in the graphitized carbon layers [39]. When carbon atoms in the graphitized carbon layers were replaced by nitrogen atoms and became "graphitic" nitrogen, the corresponding peak in the high-resolution N 1s spectra was located at 400.9 eV [40].

To investigate the photothermal performance of Co@NCNTs/Si pillars, Si pillars and Si plane were also synthesized as contrast samples. As shown in Fig. 3a, the wafer-sized silicon with the diameter of 35 mm, possessed the evenly distributed pores with the diameter of 1 mm. From the picture of Co@NCNTs/Si pillars under sunlight, the pores on the silicon chip were uniform and transparent in Fig. S6 (Supporting information). The photothermal transformation of Co@NCNTS/Si pillars was an indispensable capability for the solar-thermal water evaporation. The UV–vis

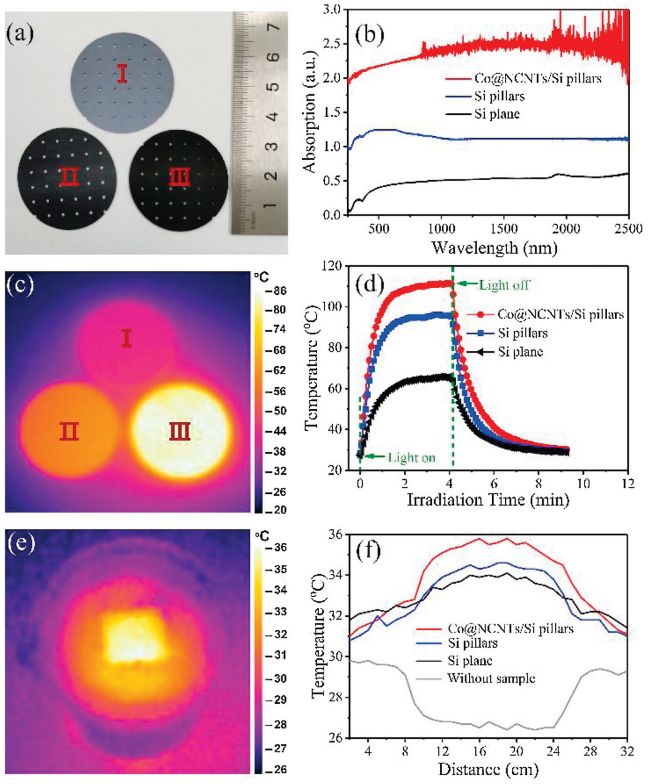

Fig. 3. (a) Photographs of (I) Si plane, (II) Si pillars, (III) Co@NCNTs/Si pillars and (b) UV–vis-NIR absorption spectra of three samples. (c) IR images of (I) Si plane, (II) Si pillars, (III) Co@NCNTs/Si pillars under solar simulator (1 sun AM 1.5 G). (d) The monitored surface temperature under solar simulator (1 sun AM 1.5 G). (e) IR image of Co@NCNTs/Si pillars floated on the surface of water under solar simulator (1 sun AM 1.5 G). (f) Sample surface temperature distribution during water evaporation of Si plane, Si pillars and Co@NCNTs/Si pillars under solar simulator (1 sun AM 1.5 G).

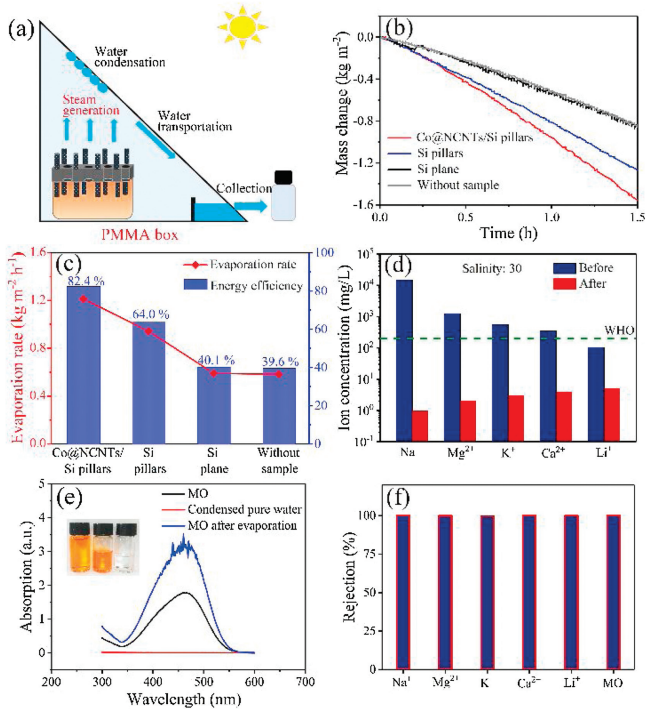

Fig. 4. (a) Schematic diagram of water evaporator. (b) Photothermal water evaporation performance of Si plane, Si pillars and Co@NCNTs/Si pillars tested by an equilibrium. (c) The corresponding evaporation rate and energy efficiency at equilibrium. (d) Comparison of the concentration of five ions in the seawater with a salinity of 30 and the collected water after evaporation. (e) Absorption spectra of methyl orange (MO) solution before evaporation (black line), the collected clean water after evaporation (red line) and the MO after evaporation (blue line) severally. Photograph embedded in (e) was the group photo of MO before evaporation (left) and the concentrated MO solution (middle), the collected clean water (right) after evaporation. (f) Metal ions and MO removal rate after the evaporation process.

absorption spectra of Si plane, Si pillars and Co@NCNTS/Si pillars were shown in Fig. 3b. As shown, the total absorption spectra in the wavelength range of 250–2500 nm for Co@NCNTs/Si pillars, Si pillars and Si plane, respectively. The highest absorption shown by the Co@NCNTs/Si pillars sample indicated that it absorbed most of the optical light in the studied range. It could be inferred that the high light capture ability of the Co@NCNTs/Si pillars sample was due to the wide light absorption range of the carbon nanotube, meanwhile, the cylindrical three-dimensional structure of the Co@NCNTs/Si pillars sample could extend the optical path and further improved the light capture ability of the sample [41,42]. The multiple refractions were performed on the surface of the Co@NCNTs/Si pillars to extend the optical path and thus enhanced the absorption of light.

To compare photothermal performance of Co@NCNTs/Si pillars, Si pillars and Si plane, infrared thermal images using a simulated sunlight irradiation (AM 1.5 G, 100 mW/cm^2) were revealed in Fig. 3c. When the light was turned on, the temperature on the surface of the samples rose hastily in 1.5 min. and exceed 80 °C. The obviously highest surface temperature of Co@NCNTS/Si pillars than Si plane and Si pillars suggested the better photothermal transformation performance. The corresponding curves of surface temperature of three samples with irradiation time were shown in Fig. 3d. The surface temperature of Co@NCNTS/Si pillars was up to 80.0 °C, relatively, the temperatures of Si plane and Si pillars were 48.9 °C and 63.9 °C severally. The above data indicated that the Co@NCNTS/Si pillars possessed an elevated photothermal transformation ability, which could cause the high temperature for the solar-thermal water evaporation.

When the Si plane, Si pillars and Co@NCNTs/Si pillars were put on the water, the according temperature distribution was detected by the IR camera, as shown in Fig. 3e, When the samples were irradiated for 150 s, the according temperature distribution curves in Fig. 3f showed that the surface temperature of the Co@NCNTs/Si pillars was the highest, reaching 38.5 °C, which was higher than the temperatures of the Si plane (33.9 °C) and Si pillars (34.3 °C). The temperature of the center without adding the sample was the lowest, reaching 26.5 °C.

As a clean and sustainable energy, the utilization of solar energy in seawater desalination and sewage purification to produce pure water has been widely concerned [43]. For this matter, a convenient, suitable pure water gathering device was assembled to assess the water purification ability of the Co@NCNTs/Si pillars, as shown in Fig. 4a. After Co@NCNTs/Si pillars was gained, the Co@NCNTs/Si pillars assembled with water evaporation appliance was performed by using Co@NCNTs/Si pillars. When the Co@NCNTs/Si pillars sample as photothermal layer, was irradiated by simulated sunlight, the sample transferred the heat from photothermal conversion to the water surface. Water evaporated in the form of water vapor, and the water vapor was then condensed and collected as clean fresh water.

In order to evaluate the evaporation performance of the Co@NCNTs/Si pillars, the mass change was recorded by an electronic analytical equilibrium connected to a computer under simulated solar irradiation with the light intensity kept at 1 kW/m^2 (one sun) The corresponding energy efficiency (η) for solar to steam generation can then be calculated using the following Eq. 2 [44]:

$$\eta = (m \times h_V)/(C_{opt} \times P_o) \quad (2)$$

where m was the calibrated mass change rate under solar illumination, hv was the water vaporization enthalpy, P_o was the solar irradiation density (1 kW/m^2), and C_{opt} was the optical concentration on the evaporator surface.

As shown by the results in Figs. 4b and c, when there was no sample set on the sea water, the evaporation rate was about 0.59 kg m^{-2} h^{-1} and solar-vapor conversion efficiency reached 39.6%. When the Si pillars sample was set on the surface of the water, the water evaporation rate reached up to 0.94 kg m^{-2} h^{-1}, and solar-vapor conversion efficiency reached 64.0% in a controlled period of time, about 1.6 times the value obtained by Si plane which was without the three-dimensional pillars array structure (about 0.59 kg m^{-2} h^{-1}, 40.1%). With the help of the layer of carbon nanotubes, water evaporated at a faster rate. The Co@NCNTs/Si pillars could realize the highest evaporation rate of about 1.21 kg m^{-2} h^{-1} and highest energy efficiency of about 82.4%. The above results showed that the evaporation rate of water was improved more easily with the assistance of carbon nanotube layer. In conclusion, both the silicon pillars and the carbon tubes structure contributed to the excellent photothermal and water evaporative properties of the final sample (Co@NCNTs/Si pillars).

As shown in Fig. S7 (Supporting information), The IR camera was also used to record the time-dependent temperature profiles after the solar simulator was turned on. Next, we studied the surface temperature change of the target sample (Co@NCNTs/Si pillars) during water evaporation under the irradiation of a sun. When the lamp was not switched on, the surface temperature of the target sample in the water was 28 °C. When the lamp was switched on, the surface temperature of the sample rose to 31 °C in just 30 s, which indicated that the Co@NCNTs/Si pillars also had good photothermal performance in the water.

To evaluate the ability of the Co@NCNTs/Si pillars in seawater desalination, the standard seawater samples with salinity of 30 were employed (Fig. 4d). It was obvious that after desalination experiments using Co@NCNTs/Si pillars sample, the concentration of the five ions of Na^+, Mg^{2+}, K^+, Ca^{2+} and Li^+ examed by inductively coupled plasma optical emission spectroscopy (ICP-OES) was significantly reduced and the ion removal rate was more than 99.7%. At the same time, the ion concentration was under the salinity level specified by the World Health Organization (WHO) [45,46]. Hence, the Co@NCNTs/Si pillars sample was able to offer a high-efficiency solar water purification, which could not only gain pure water from seawater, but also worked well in the purification of sewage (Fig. 4e). The equipment achieved removal rates near 100% for ions and MO dye in dummy sewage and seawater (Fig. 4f). These results clearly showed the potential of the Co@NCNTs/Si pillars sample for solar application in the area of efficient water treatment.

In summary, a controllable method to construct photothermal three-dimensional composite combining silicon pillars and carbon nanotubes was developed in this work for highly efficient solar-driven evaporation. The three-dimensional silicon pillars could enhance the light absorbability and the layer Co@NCNTs covering on silicon pillars was a kind photothermal material with wide spectral absorption range. The above factors enabled achieving effective photothermal water evaporation. The energy efficiency could come to 82.4% without additional thermal management accessories. Therefore, this work confirmed that the 3D Co@NCNTs/Si pillars architecture had outstanding photothermal conversion ability, and had a broad application prospect in the field of using solar energy to generate steam to solve water shortage crisis.

Declaration of competing interest

The authors declare that they have no known competing financial interests or personal relationships that could have appeared to influence the work reported in this paper.

Acknowledgments

This work was supported by Taishan Scholars Project Special Funds (No. tsqn201812083), Natural Science Foundation of Shandong Province (Nos. ZR2019YQ20, 2019JMRH0410), and the National Natural Science Foundation of China (Nos. 51972147, 52022037).

Appendix A. Supplementary data

Supplementary material related to this article can be found, in the online version, at doi:https://doi.org/10.1016/j.cclet.2021.02.056.

References

[1] G. Ni, G. Li, S.V. Boriskina, et al., Nat. Energy 1 (2016) 16126.
[2] Q. Ma, P. Yin, M. Zhao, et al., Adv. Mater. 31 (2019) 1808249.
[3] Y. Yang, H. Zhao, Z. Yin, et al., Mater. Horiz. 5 (2018) 1143–1150.
[4] N.S. Lewis, Science 351 (2016) aad1920.
[5] L. Cui, P. Zhang, Y. Xiao, et al., Adv. Mater. 30 (2018) 1706805.
[6] Y. Shi, R. Li, Y. Jin, et al., Joule 2 (2018) 1171–1186.
[7] H. Ren, M. Tang, B. Guan, K. Wang, et al., Adv. Mater. 29 (2017) 1702590.
[8] N. Xu, J. Li, Y. Wang, et al., Sci. Adv. 5 (2019) eaaw7013.
[9] X. Zhou, F. Zhao, Y. Guo, et al., Energy Environ. Sci. 11 (2018) 1985–1992.
[10] H. Yuan, F. Liu, G. Xue, et al., Appl. Catal. B: Environ. 283 (2021) 119647.
[11] Y. Liu, F. Liu, N. Ding, et al., Chin. Chem. Lett. 31 (2020) 2539–2548.
[12] G. Wang, Y. Fu, X. Ma, et al., Carbon 114 (2017) 117–124.
[13] W. Zhong, Y. Zhang, L. Zhao, et al., Chin. Chem. Lett. 31 (2020) 2651–2656.
[14] X. Pan, J. Ji, N. Zhang, et al., Chin. Chem. Lett. 31 (2020) 1462–1473.
[15] X. Zhang, W. Gao, X. Su, et al., Nano Energy 48 (2018) 481–488.
[16] H. Wu, H. Tan, L. Chen, et al., Chin. Chem. Lett. 32 (2021) 2499–2502.
[17] Y. Wang, C. Wang, X. Song, et al., J. Mater. Chem. A 6 (2018) 963–971.
[18] C. Chen, Y. Li, J. Song, et al., Adv. Mater. 29 (2017) 1701756.
[19] Y. Kuang, C. Chen, S. He, et al., Adv. Mater. 31 (2019) 1900498.
[20] P. Zhang, Q. Liao, T. Zhang, et al., Nano Energy 46 (2018) 415–422.
[21] C.M. Das, L. Kang, Q. Ouyang, et al., InfoMat 2 (2020) 698–714.
[22] Z. Li, C. Wang, Chin. Chem. Lett. 31 (2020) 2159–2166.
[23] J. Tang, T. Zheng, Z. Song, et al., ACS Appl. Mater. Interfaces 12 (2020) 18504–18511.
[24] P. Fan, H. Wu, M. Zhong, et al., Nanoscale 8 (2016) 14617–14624.
[25] P. Fan, B. Bai, M. Zhong, et al., ACS Nano 11 (2017) 7401–7408.
[26] L. Zhou, Y. Tan, J. Wang, et al., Nat. Photonics 10 (2016) 393–398.
[27] G. Xiong, J. Jia, L. Zhao, et al., Sci. Bull. 66 (2021) 386–406.
[28] A. Wang, L. Zhao, J. Yu, et al., Int. J. Hydrogen Energy 43 (2018) 9279–9286.
[29] M. Kumar, Y. Ando, J. Nanosci, Nanotechnology 10 (2010) 3739–3758.
[30] J. Peng, Y. He, C. Zhou, S. Su, B. Lai, Chin. Chem. Lett. 32 (2021) 1626–1636.
[31] B. Liu, H. Zhou, H. Jin, et al., Chin. Chem. Lett. 32 (2021) 535–538.
[32] E.O. Pentsak, E.G. Gordeev, V.P. Ananikov, ACS Catal. 4 (2014) 3806–3814.
[33] J. Yu, G. Li, H. Liu, et al., Adv. Sci. 6 (2019) 1901458.
[34] F. Liu, J. He, X. Liu, et al., Carbon Energy 3 (2021) 129–141.
[35] N. Yang, Z.X. Luo, G.R, et al., ACS Appl. Mater. Interfaces 11 (2019) 35987–35998.
[36] J. Bae, D.S. Kim, H. Yoo, et al., ACS Appl. Mater. Interfaces 8 (2016) 4541–4547.
[37] G. Zheng, Y. Xiang, L. Xu, et al., Adv. Energy Mater. 8 (2018) 1801718.
[38] Z. Yang, C. Zhao, Y. Qu, et al., Adv. Mater. 31 (2019) 1808043.
[39] M.S. Jo, J.S. Lee, S.Y. Jeong, et al., Small 16 (2020) 2003391.
[40] Z.H. Sheng, L. Shao, J.J. Chen, et al., ACS Nano 5 (2011) 4350–4358.
[41] A. Kousalya, C. Hunter, S. Putnam, T. Miller, T. Fisher, Appl. Phys. Lett. 100 (2012) 071601.
[42] P. Fan, B. Bai, J. Long, et al., Nano Lett. 15 (2015) 5988–5994.
[43] Z. Xin, X. Zhao, H. Ji, et al., Chin. Chem. Lett. 32 (2021) 2151–2154.
[44] H. Ghasemi, G. Ni, A.M. Marconnet, et al., Nat. Commun. 5 (2014) 4449.
[45] F. Zhao, X. Zhou, Y. Shi, et al., Nat. Nanotechnol. 13 (2018) 489–495.
[46] X. Zhao, X.J. Zha, J.H. Pu, et al., J. Mater. Chem. A 7 (2019) 10446–10455.